Chemical Engineering Research and Design 236 (2026) 485–494

Contents lists available at ScienceDirect

Chemical Engineering Research and Design

journal homepage: www.elsevier.com/locate/cherd

Parametric modelling and cost optimisation of ethylene degradation via vacuum-ultraviolet photolysis

Buntu Godongwana [a,*], Nina Mntwini [b], Bongolwetu Mabusela [c], Patricia Mathabe [d]

[a] Department of Chemical and Materials Engineering, University of South Africa, Private Bag X6, FL 1710, South Africa
[b] Department of Chemical Engineering, Cape Peninsula University of Technology, PO Box 1906, Bellville 7535, South Africa
[c] Department of Chemical Engineering, University of Johannesburg, PO Box 17011, Doornfontein 2028, South Africa
[d] School of Agriculture, Food and Environment, Royal Agricultural University, Cirencester GL7 6SJ, United Kingdom

ARTICLE INFO

Keywords:
Ethylene Oxidation
VUV Photolysis
Parametric Optimisation
Box-Behnken Design
Spoilage Coefficient

ABSTRACT

The current study develops a coupled mass and energy balance model for a batch VUV photolysis reactor for the oxidation of ethylene. The input variables are expressed in terms of dimensionless groups. The direct oxidation assumption often used in literature is shown to be a limiting case of indirect oxidation, based on the quasi-steady-state assumption. The resulting system of non-linear differential equations is solved numerically using MATLAB®. Using apple storage as a case study, for the single operating conditions used for quantitative validation (9 W and 90% relative humidity), the model describes the measured temperature response with $R^2 = 0.909$. The conversion model captures the qualitative progression of degradation but underpredicts conversion at longer reaction times ($R^2 = 0.754$). The model does not incorporate the effects of hydroxyl radicals produced by the photodissociation of water molecules by ultraviolet light, and therefore does not explicitly represent the impact of humidity or the additional reactions driven by these radicals. A Box-Behnken response surface methodology is used to correlate the effect of relative humidity (0 – 90%), light intensity (3 – 9 W), initial concentration (5 – 50 ppm) to the percentage removal and to estimate the optimisation conditions. A parametric cost optimisation framework is proposed to identify the optimal lamp power that minimises the combined cost of electricity and ethylene-related fruit spoilage. The results demonstrate a trade-off between conversion efficiency and energy consumption. An ideal minimum cost of ethylene treatment was determined for a specified lamp wattage. The developed model provides a quantitative basis for the design and economic evaluation of VUV photolysis systems in postharvest fruit handling applications.

1. Introduction

Fruit production is reported to account for 10% of the global produce of primary crops (FAO., 2024), and climacteric fruits can be estimated to constitute between 30% and 50% of this value. The classification of fruits as climacteric or non-climacteric is based on their ripening behaviour, with climacteric fruits (bananas, apples, avocados, pears, *etc.*) characterised by their continued metabolic activity and ethylene (C_2H_4) production after harvesting (Nasir et al., 2024). Ethylene in plants acts as a natural ripening hormone responsible for accelerating senescence and is synthesized by the two enzymes: 1-Aminocyclopropane-1-carboxylic acid synthase and 1- Aminocyclopropane-1-carboxylic acid oxidase (Khan et al., 2024). The food waste and economic losses due to C_2H_4 on climacteric fruits has been estimated to be as high as 80% of their market value (Keller et al., 2013). Vacuum ultraviolet (VUV) photolysis has emerged as a promising advanced oxidation process for the degradation of C_2H_4 at low-concentrations, particularly in controlled environments where rapid and residue-free decomposition is critical (Pathak et al., 2019). The inherent advantage of VUV photolysis is the production of ozone which results in high removal efficiencies compared to conventional thermal or chemical oxidation technologies (Chen et al., 2010). Chemical oxidation systems require large quantities of absorbent material (Keller et al., 2013); while catalytic systems are capital intensive, and generally produce lower oxidation rates due to competitive or weak adsorption of the reactants on the surface of the catalyst (Ray, 2000; Pathak and Mahajan, 2017; Soneji et al., 2024). Despite its effectiveness, the practical implementation of VUV photolysis may be constrained by operational costs for sustained power demand of the VUV

* Corresponding author.
E-mail address: godonb@unisa.ac.za (B. Godongwana).

https://doi.org/10.1016/j.cherd.2026.11.031
Received 18 December 2025; Received in revised form 15 October 2026; Accepted 11 November 2026
Available online 17 November 2026
0263-8762/© 2026 The Author(s). Published by Elsevier Ltd on behalf of Institution of Chemical Engineers. This is an open access article under the CC BY license (http://creativecommons.org/licenses/by/4.0/).

lamps. The operational costs of photodegradation have been reported to be higher than that of biological treatments, for the same effect, however these are often very slow (Chen et al., 2010). Previous experimental studies have shown an increase in C_2H_4 oxidation rates with increased UV light intensity (Pathak et al., 2017; Mabusela et al., 2024). However, the UV lamps consume significant electrical energy per order (E_{EO}) at low intensities to maintain the required photon flux (Mabusela et al., 2024). It is therefore important to identify and optimise key reactor parameters that influence both degradation efficiency and energy consumption.

The complete modelling of the VUV process involves the simultaneous resolution of the conservation equations of mass, momentum, and radiative energy, together with the appropriate kinetic model (Bagheri and Mohseni, 2014). The mechanisms and kinetics of VUV-induced photodegradation of various compounds has been thoroughly studied, from a theoretical and experimental perspective. Chen et al. (2010) investigated VUV photodegradation of gaseous α-pinene in a spiral reactor, examining how reaction medium and residence time affect intermediate formation and biodegradability. A detailed mechanistic model incorporating chemical kinetics and flow dynamics was developed by Asili and De Visscher (2014) to simulate UV-induced degradation of H_2S in waste gas, accurately predicting major products and reaction efficiencies. They also developed a similar model for the degradation of methane and ethane (Asili and de Visscher, 2018). Mahmoudkhani et al. (2016) simulated UV and UV/O_3-induced degradation of gaseous benzene in a photochemical reactor, achieving 70% removal efficiency. The model accurately predicted reactor performance and confirmed a synergistic enhancement of degradation efficiency in the presence of ozone. Xu et al. (2018) developed a VUV model for degradation of H_2S in the absence of O_2. Their model also included a three-dimensional light intensity distribution model in the reactor. Pathak et al. (2019) compared the relative efficacies of C_2H_4 removal by VUV photolysis versus photocatalytic oxidation (PCO). Their results showed higher rates of C_2H_4 degradation in VUV photolysis compared to PCO. The VUV photolysis was shown to follow first-order kinetics with respect to C_2H_4 concentration, while Mabusela et al. (2024) has shown that the order of reaction is a strong function of the light intensity. A recent study by Farkas et al. (2024) comparing UV (254 nm), UV/VUV (254/185 nm), and ozonation-based processes highlights the growing focus on combining photolytic and oxidative pathways to achieve faster transformation and safer effluents in VUV-based photodegradation systems.

Although extensive research has focused on mathematical modelling of VUV photolysis for predicting degradation efficiency, limited attention has been given to energy balance models that account for temperature variations in the reactor caused by heat from VUV lamps and chemical reactions. Such temperature rise can significantly influence degradation performance, as was reported by Pathak et al. (2017). Furthermore, existing studies lack analytical evaluations of the reactor's economic feasibility through parametric optimisation. This study aims to address these gaps in current VUV reactor modelling for industrial application.

2. The VUV model development

2.1. The VUV reactor

The model presented in this paper is applicable to a vacuum ultraviolet photolysis reactor, with UV lamps mounted on the inside of the reactor. The construction of the reactor is illustrated in Fig. 1. The VUV light source is a low-pressure mercury lamp with approximately 85% output at wavelength $\lambda = 254$ nm and 15% output at $\lambda = 185$ nm. The reactor is constructed from stainless steel and the lid constructed from borosilicate glass and features openings for VUV lamp fittings and a temperature and humidity sensor. The C_2H_4-air mixture is introduced into the reactor through the inlet port. An external circulation line connects the reactor outlet to an ethylene analyser (Fricaval89 SL, Valencia-Spain), allowing gas to be withdrawn for ethylene concentration measurements and subsequently returned to the reactor, as shown in Fig. 1. The dimensions and operating conditions of the reactor are listed in Table 1.

2.2. Model assumptions

The model is based on the following assumptions: (1) at moderate oxygen concentrations the oxidation of C_2H_4 occurs indirectly via highly reactive intermediates. The C_2H_4 absorption of electromagnetic radiation of $\lambda = 185$ nm is weak in comparison with O_2, which is generally available at much higher concentrations in storage environments. At this wavelength, the photolysis of C_2H_4 will result from the photodissociation of O_2. However, in pure nitrogen environments (or very low O_2 concentration) the $\lambda = 254 + 185$ nm irradiated UV photons will be absorbed directly by the C_2H_4 molecules. Nitrogen has been reported not to absorb photons with wavelengths exceeding 120 nm (Wang and Ray,

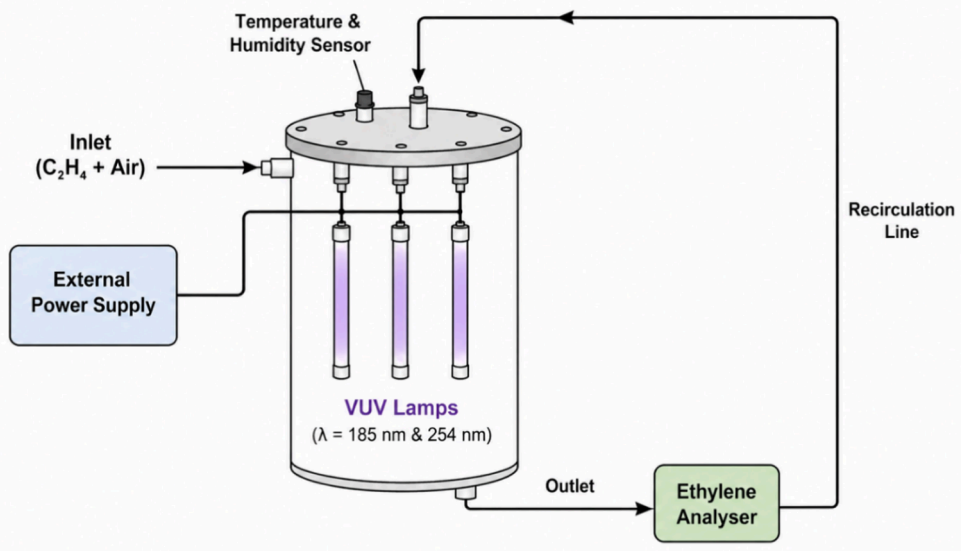


Fig. 1. A schematic of the VUV photolysis experimental setup, showing the VUV lamps (185 and 254 nm), reactor chamber, and external gas recirculation loop connected to the ethylene concentration analyser.

Table 1
Model input parameter values for the VUV photolysis of ethylene.

Description	Parameter	Value	Units
Initial concentration	c_{A0}	51	ppm
Ambient air temperature	T_0	298.15	K
Reactor pressure	P_0	101.325	kPa
Reactor length	L	0.22	m
Reactor diameter	D	0.12	m
Lamp length	L_e	0.052	m
Lamp diameter	D_e	0.017	m
Density of gas mixture	ρ	1.184	kg m^{-3}
Viscosity of gas mixture	μ	1.85×10^{-5}	Pa.s
Density of lamp	ρ_e	2500	kg m^{-3}
Heat capacity of gas mixture	c_p	1005	J kg^{-1}K^{-1}
Heat capacity of lamp	c_{pe}	750	J kg^{-1}K^{-1}
Thermal conductivity of mixture	κ	0.0262	W m^{-1}K^{-1}
Thermal expansion of mixture	φ	0.003354	K^{-1}
Heat transfer coefficient	h_e	30	W m^{-2}K^{-1}
Power rating of UV lamp	Φ	9	W
UV light intensity	I_0	0.012	mW cm^{-2}
Lamp emissivity	ϵ	1	-

2000; Chang et al., 2013). Under these conditions the photolysis therefore can be assumed to be dominated by direct oxidation; (2) the pseudo-homogenous assumption neglects internal and external mass transfer limitations. The reactor operates entirely in the gas phase, at low ethylene concentrations (5 – 50 ppm), where intermolecular interactions are minimal and gas-diffusivities are high. Furthermore, the Rayleigh numbers ($N_{Ra} \approx 10^4$ - 10^6) indicate strong natural convection and reduced concentration gradients; (3) the primary and immediate products of ozonolysis of C_2H_4 are formaldehyde and formic acid; (4) constant density system; (5) C_2H_4-air physical properties are approximated using properties of air, this is due to the low concentrations of C_2H_4; (6) the reactor is treated as a spatially lumped, well-mixed batch gas phase. Internal mixing is assumed to be sufficiently rapid relative to the characteristic reaction time, with buoyancy driven natural convection providing the principal mixing mechanism.

3. Mathematical formalism

3.1. Mass and energy balances

The indirect oxidation of C_2H_4 uses highly reactive intermediates O and O_3 to degrade C_2H_4 according to the following reactions (Warneck, 1988; Jozwiak et al., 2000; Huang et al., 2016):

$$O_2 + h\nu(185nm) \rightarrow O(^1D) + O(^3P) \quad (1a)$$

$$O_2 + O(^1D) + M \rightarrow O_3 + M \quad (1b)$$

$$O_3 + h\nu(254nm) \rightarrow O_2 + O(^1D) \quad (1c)$$

$$O_3 + O(^1D) \rightarrow O_2 + O_2 \quad (1d)$$

$$O(^1D) + C_2H_4 \rightarrow Products \quad (1e)$$

$$O_3 + C_2H_4 \rightarrow Products \quad (1f)$$

Where M denotes the inert N_2. The corresponding rate equations are as follows (Jozwiak et al., 2000):

$$\frac{dc_D}{dt} = 2j_0c_C - k_2c_Dc_Cc_M + j_1c_B - k_4c_Dc_B - k_5c_Dc_A \quad (2a)$$

$$\frac{dc_C}{dt} = -j_0c_C - k_2c_Dc_Cc_M + j_1c_B + 2k_4c_Dc_B \quad (2b)$$

$$\frac{dc_B}{dt} = k_2c_Dc_Cc_M - j_1c_B - k_4c_Dc_B - k_6c_Bc_A \quad (2c)$$

$$\frac{dc_A}{dt} = -k_5c_Dc_A - k_6c_Bc_A \quad (2d)$$

Where c_A, c_B, c_C, c_D, c_M represents the concentrations of the chemical species C_2H_4, O_3, O_2, O, and N_2, respectively; k_i the chemical reaction rate constant for the i^{th} reaction in the reaction system; j_0 and j_1 the photodissociation coefficients of O_2 ($\lambda = 185$ nm) and O_3 ($\lambda = 254$ nm), respectively. The coefficient j is dependent on the intensity of solar radiation and the photo-physical properties of the absorbing molecule and is given by (Klöpffer and Wagner, 2007):

$$j = \int_{\lambda_1}^{\lambda_2} \sigma(\lambda)\phi(\lambda)I(\lambda)d\lambda \quad (3)$$

Where $I(\lambda)$ is the spectral photon irradiance (photons cm^{-2} min^{-1} nm^{-1}); $\sigma(\lambda)$ the absorption cross-section (cm^2 molecule^{-1}); $\phi(\lambda)$ the quantum yield (number of oxidized molecules per photon absorbed). Making use of the quasi-steady-state assumption for the highly reactive O species (i.e. $\frac{dc_D}{dt} = 0$), it follows that:

$$\frac{dc_A}{dt} = -k_5c_A\left[\frac{2j_0c_C + j_1c_B}{k_2c_Mc_C + k_4c_B + k_5c_A}\right] - k_6c_Bc_A \quad (4)$$

The yield of O_3 from VUV irradiation has been reported to be very low, ranging between 7.2 g/kWh and 9 g/kWh for air and oxygen, primarily because of decomposition by 254 nm UV light (Keller et al., 2013; Huang et al., 2016). This yield may decrease even lower with lamp aging due to reduced photon emission at 185 nm, or vary with oxygen concentration. A lower ozone yield would reduce the contribution of indirect oxidation pathways, thereby shifting the system toward direct photolysis. Eq. (4) therefore reduces to:

$$\frac{dc_A}{dt} = -\frac{2j_0c_Ac_C}{\left(\frac{k_2c_M}{k_5}\right)c_C + c_A} \quad (5)$$

The constant k_2 has weak temperature dependence, since the recombination reaction of Eq. (1b) does not require activation energy (Warneck, 1988). The direct photolysis assumption is therefore a limiting case of Eq. (5), in oxygen-rich environments, when $c_C \gg c_A$, to give:

$$\frac{dc_A}{dt} = -\left(\frac{2k_{50}}{k_2c_M}\right)j_0e^{-(E_5)/RT}c_A \quad (6)$$

Where k_{50} is the Arrhenius pre-exponential factor for the decomposition reaction of Eqn (1e), and E_5 is the corresponding activation energy. The constant value in parenthesis in Eq. (6) can be arbitrarily put equal unity without loss of generality. The model will be expressed in terms of ethylene conversion x_A, with the relationship between conversion and concentration given by (Levenspiel, 1998):

$$c_A = c_{A0}\frac{1 - x_A}{1 + \varepsilon_A x_A}\left(\frac{T_0}{T}\right) \quad (7)$$

Where c_{A0} is the initial concentration of ethylene; ε_A is the fractional change in volume of the system; T_0 and T are the initial and variable temperatures of the system, respectively. Eq. (6) is made dimensionless

by introducing the following dimensionless variables for a constant density system (i.e $\varepsilon_A = 0$):

$$\tau = k_0 t; \theta = \frac{T}{T_0}; \psi = \frac{T_e}{T_0}; \zeta_5 = \frac{E_5}{RT_0}; \Pi_0 = \frac{j_0}{k_0} \tag{8}$$

Where $k_0 = k_2 c_M c_{A0}$. Substituting the dimensionless variables in Eq. (8) into Eq. (6) results in:

$$\frac{dx_A}{d\tau} = \Pi_0 e^{-\zeta_5/\theta}(1 - x_A) \tag{9}$$

The energy balance of the VUV reactor is given by:

$$\rho c_p V \frac{dT}{dt} = h_e A_e (T_e - T) - h_r A_r (T - T_\infty) + \epsilon \delta A_e \left(T_e^4 - T^4\right) + V \sum_{i=1}^{6} r_i H_{rxn,i} \tag{10}$$

Where ρ is the density of the gas mixture; c_p is the specific heat capacity of the gas mixture; V is the volume of the reactor; h_e and h_r are the heat transfer coefficients on the external surfaces of the lamp A_e and reactor A_r, respectively; T_e is the temperature of the lamp; ϵ is the emissivity of the lamp; δ is the Stefan-Boltzmann constant; $H_{rxn,i}$ is the heat of reaction of the i^{th} reaction and r_i is the corresponding rate of reaction. Eq. (10) is made dimensionless by introducing the following dimensionless variables:

$$N_{st} = \frac{h}{\rho c_p u}; \Lambda = \frac{\epsilon \delta T_0^3}{\rho c_p u}; \Omega_i = \frac{r_i}{k_0}\left(\frac{H_{rxn,i}}{\rho c_p T_0}\right); \vartheta = \frac{A_e u}{V k_0} \tag{11}$$

Where u is the buoyant velocity, given by:

$$u = \sqrt{g\varphi(T_e - T_\infty)L_e} \tag{12}$$

Where φ is the thermal expansion coefficient, L_e is the length of the VUV lamp, and g is gravitational acceleration. Substituting the dimensionless variables in Eq. (11) into Eq. (10) gives:

$$\frac{d\theta}{d\tau} = \vartheta\left[N_{St}^e(\psi - \theta) - N_{St}^r(\theta - 1) + \Lambda\left(\psi^4 - \theta^4\right)\right] + \sum_{i=1}^{6} \Omega_i \tag{13}$$

The reaction parameter Ω and corresponding constants are given in Appendix A. The dimensionless energy balance of the VUV lamp is given by:

$$\frac{d\psi}{d\tau} = \Gamma_{uv} - \Upsilon(\psi - \theta) - \quad \eta\left(\psi^4 - \theta^4\right) \tag{14}$$

With the introduction of the additional dimensionless variables:

$$\Gamma_{uv} = \frac{\Phi}{m_e c_{pe} k_0 T_0}; \Upsilon = \frac{h_e A_e}{m_e c_{pe} k_0 T_0}; \eta = \frac{\epsilon \delta A_e T_0^3}{m_e c_{pe} k_0} \tag{15}$$

Where Φ is the power rating of the UV source; m_e is the mass of the lamp; and c_{pe} is the specific heat capacity of the lamp. The input values required to solve Eqs. (9), (13) and (14) are listed in Table 1 and Table 2. The Stanton number N_{St} correlation for natural convection adjacent to a vertical lamp, in Eq. (13), is given by Churchill and Chu (Popiel, 2008):

$$N_{st} = \frac{1}{N_{Pe}}\left[0.68 + \frac{0.67 {N_{Ra}}^{1/4}}{\left(1 + (0.492/N_{\mathrm{Pr}})^{9/16}\right)^{4/9}}\right] N_{Ra} < 10^9 \tag{16}$$

Where N_{Pe} is the Peclet number, N_{Ra} is the Rayleigh number, and N_{Pr} the Prandtl number, respectively given by:

$$N_{Pe} = \frac{uL_e}{\gamma}; N_{Ra} = \frac{\rho u^2 L_e^2}{\gamma \mu}; N_{\mathrm{Pr}} = \frac{c_p \mu}{\kappa} \tag{17}$$

Where μ is the dynamic viscosity, γ the thermal diffusivity, and κ is the thermal conductivity. Eqs. (9) - (14) are not amenable to analytical solutions and require a numerical solver. The equations will be solved using the *ode45* numerical solver on MATLAB®.

Table 2
Rate coefficients and activation energies for the VUV photolysis of ethylene.

Parameter	Value	Units	Reference
k_0	14.56	s^{-1}	-
k_2	203.081	$m^6\ mol^{-2}\ s^{-1}$	Warneck, 1988; Atkinson et al., 2004
k_4	4.818×10^3	$m^3\ mol^{-1}\ s^{-1}$	Warneck, 1988
k_5	4.878×10^5	$m^3\ mol^{-1}\ s^{-1}$	Atkinson, 1997
k_6	0.964	$m^3\ mol^{-1}\ s^{-1}$	Atkinson et al., 2006
E_4/R	2.060×10^3	K	Warneck, 1988; Atkinson, 2004
E_5/R	800 ± 200	K	Cvetanović, 1987
E_6/R	2.580×10^3	K	Atkinson et al., 2006
σ_0 (O_2, 185 nm)	3.3×10^{-20}	cm^2 molecule^{-1}	Atkinson et al., 2004
σ_1 (O_3, 254 nm)	1147×10^{-20}	cm^2 molecule^{-1}	Atkinson et al., 2004
$\phi_0\left[O(^3P), 185nm\right]$	1	-	Atkinson et al., 2004
$\phi_1\left[O(^1D), 254nm\right]$	0.9	-	Atkinson et al., 2004
$\Delta H^\circ_{rxn,1}$	494	kJ mol^{-1}	Atkinson et al., 2004
$\Delta H^\circ_{rxn,3}$	448	kJ mol^{-1}	Atkinson et al., 2004
$\Delta H^\circ_{rxn,4}$	-393.0	kJ mol^{-1}	Atkinson et al., 2004
$\Delta H^\circ_{rxn,5}$	-350 ± 200	kJ mol^{-1}	-
$\Delta H^\circ_{rxn,6}$	-690	kJ mol^{-1}	-

3.2. Empirical modelling

The mass and energy conservation models of Eqs. (9) – (14) do not account for the effect of relative humidity (RH) on the percentage ethylene removal (PER) in the reactor. A number of studies have shown that the indirect oxidation of organic compounds is a function of the concentration of the hydroxyl radicals resulting from the photodissociation of water molecules by ultraviolet light (Feiyan et al., 2002; Cheng et al. 2011; Asili, de Visscher, 2014; Pathak et al. 2017). The appropriate kinetic expression which accounts for the concentration of hydroxyl radicals is still a subject of research (Mabusela et al. 2022). Accordingly, a Box-Behnken design of experiment (DOE) methodology was used to develop an empirical correlation between the process variables and the PER. The main variables investigated were RH (0 – 90%), VUV lamp power (3 – 9 W), and initial C_2H_4 concentration (5–50 ppm). The second-order equation was developed through STAT-EASE 360, and the correlation in terms of coded values of the variables is given by:

$$PER = \beta_0 + \sum \beta_i x_i + \sum \beta_{ij} x_i x_j + \sum \beta_{ij} x_i^2 \tag{18}$$

Where *PER* is the response corresponding to the independent variables x_i and x_j; β_0, β_i $(i = 1, 2, 3; j = 1, 2, 3)$ are the coefficients of the response model. It is important to emphasize that the RSM model does not replace the mechanistic formulation presented in Section 3.1, but rather complements it. While the mechanistic model captures the fundamental photochemical kinetics under dry conditions, the RSM framework quantifies additional humidity-driven pathways, particularly radical (·OH) mediated oxidation, that are not explicitly represented in the current kinetic scheme.

3.3. Parametric cost optimisation model

The numerical solution of Eqs. (9) - (14) are presented in Section 4 and demonstrate that operating the VUV lamp at low wattage requires a relatively long operating time to reach the final conversion values. These results immediately present an optimization challenge: what UV lamp power is required to minimise the running costs of electricity while

maintaining an acceptable rate of conversion of the ethylene? The objective function for the optimization is therefore:

$$\min_{P} C_{total} = C_{elec}(\Phi) + C_{unreacted}(\Phi) \tag{19}$$

$$C_{elec} = \omega \bullet \Phi \bullet t_{batch} \tag{20}$$

$$C_{unreacted} = \varpi \bullet [1 - x_A(\Phi)] \bullet c_{A0}(ppm) \tag{21}$$

Where ω is the unit cost of electricity (R/kWh); ϖ is the cost of unreacted ethylene (R/ppm C_2H_4); $x_A(\Phi)$ is the conversion as a function of lamp power.

The cost of unreacted ethylene ϖ is derived by linking ethylene concentration to fruit spoilage via the spoilage coefficient k_s,as follows:

$$\frac{[TSS/TA]_{t1} - [TSS/TA]_{t0}}{[TSS/TA]_{t0}} = k_s[C_2H_4] \tag{22}$$

Where the total soluble solids to titratability acidity ratio (TSS/TA) is a key maturity and quality index for measuring the ripening rate of climacteric fruits. The current authors (Mabusela et al., 2024) have reported a 42% increase in the TSSA/TA over a period of 28 days, with an ethylene generation rate of 6.66 μL/kgh for apples stored under the conditions considered in this study (Mabusela et al.,2023). This corresponds to an effective spoilage coefficient of $k_s = 0.00028$ ppm-^{1}. Multiplying this by the estimated loss per unit mass for fruit (m_v = R20/kg) in Table 3, yields a cost factor of R0.0056 per ppm of unreacted ethylene. This formulation assumes a linear relationship between ethylene concentration and spoilage rate within the investigated range. The unit of electricity was based on the average cost of commercial electricity in South Africa at the time of writing (R4.60/kWh).

4. Results

4.1. Model validation and thermal-kinetic response

The coupled mass-energy balance model was validated against experimental data for temperature and ethylene conversion, at one operating condition (9 W and 90% RH), and the results are presented in Figs. 2 and 3, respectively. The model achieved good agreement with temperature experiments, yielding $R^2 = 0.909$. The conversion model reproduces the qualitative progression of ethylene degradation and provided reasonable agreement during the initial and intermediate conversion regimes; however, underprediction becomes evident at high conversion, resulting in an R^2 of 0.754. The discrepancy between the model and experiment indicates that the O/O_3-based reaction mechanism does not fully represent the oxidation pathways occurring under the experimental conditions. This is particularly relevant because the validation experiment was conducted at 90% RH. Water-vapour photolysis can generate hydroxyl radicals that participate in parallel oxidation reactions. Since ·OH concentration was not measured in the present experiments, an explicit ·OH mechanism cannot be formulated. The observed deviation is therefore interpreted as evidence of an additional humidity-dependent reaction contribution.

The Stanton number was found to be a key determinant of thermal response. In Fig. 2, $N_{St}^r = 0.0061$ corresponds with the assumption of negligible heat losses to the surroundings. Increasing the Stanton number from $N_{St} = 0.0061$ to $N_{St} = 0.0916$ improved correlation with measured data, confirming that convective heat losses from the lamp surface substantially influence the reactor temperature profile. Fig. 4(b) and (d) illustrate the temperature rises of both the lamp and the reactor environment. An increase in lamp wattage from 6 W to 12 W results in a corresponding increase in both the nearly parallel profiles.

The inclusion of the energy balance distinguishes this model from previous kinetic-only models (Asili and de Visscher, 2018; Xu et al., 2018). The observed temperature rise in Fig. 2 originates not only from lamp radiation but also from the exothermic ozonolysis of ethylene to formaldehyde and formic acid. The combination of the dimensionless groups N_{Ra}, N_{Pr}, and N_{St} provides a compact description of heat-transfer behaviour, where the large N_{Ra} (1×10^4 – 1×10^6) indicate buoyancy-driven mixing that mitigates temperature stratification and improves photo-utilisation efficiency. Using air-C_2H_4 mixture properties listed in Table 1, $N_{PR} \approx 0.71$, with N_{St}^e values between 0.02 – 0.06 and heat transfer coefficients $h_e \approx 3$ – 9 W/m^{2}K.

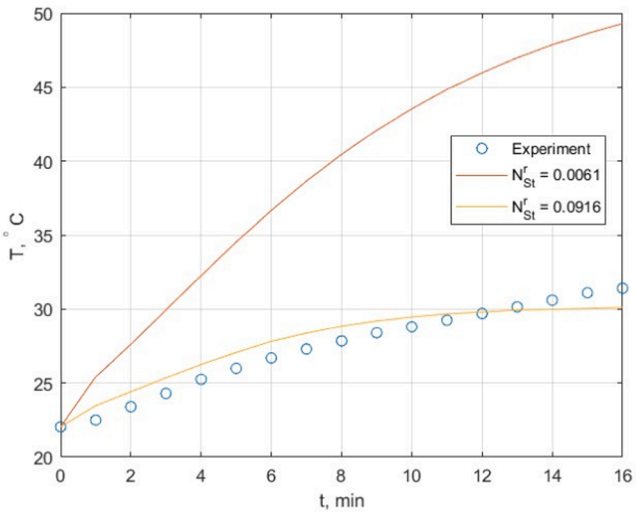


Fig. 2. Comparison of the theoretical temperature profile with experimental results (Φ = 9 W, RH = 90%).

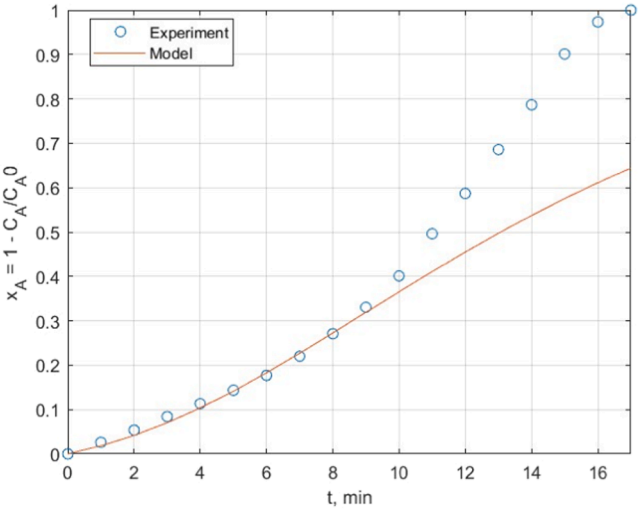


Fig. 3. Comparison of the theoretical conversion with experimental results (Φ = 9 W, RH = 90%).

Table 3
Model input parameter values for Cost optimisation.

Description	Parameter	Value	Units
Unit of electricity	ω	4.60	R/kWh
Market value of apples (golden delicious, ~200 g)	m_v	20.00	R/kg
Spoilage coefficient	k_s	0.00028	ppm^{-1}
Cost of unreacted ethylene	$\varpi = k_s m_v$	0.0056	R/ppm C_2H_4
Initial concentration of C_2H_4	c_{A0}	51.0	ppm

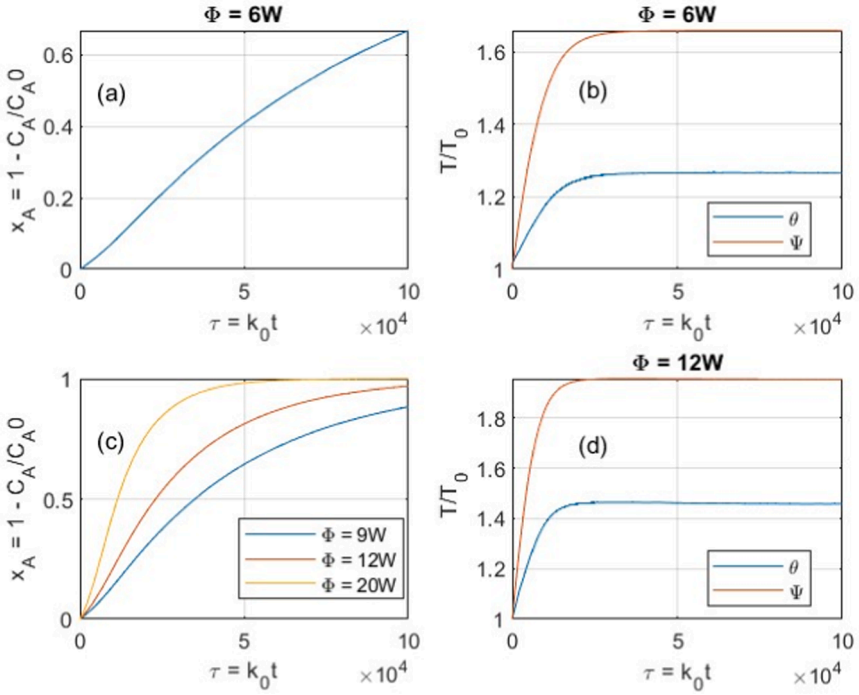


Fig. 4. Conversion of ethylene in a VUV photolysis reactor ($\Lambda = 0.003$; $N^r_{St} = 0.0916$; $N^e_{St} = 0.0183$).

4.2. Ethylene conversion

Fig. 4(a) and (c) illustrate the predicted conversion of C_2H_4 for various lamp intensities and reaction times. These figures exhibit the characteristic sigmoid shape, reflecting sequential stages of radical generation and C_2H_4 oxidation. The initial lag phase corresponds to the build-up of reactive intermediates (O and O_3) formed by O_2 photodissociation at $\lambda = 185$ nm. Once a sufficient radical concentration is established, the reaction enters an acceleration phase where oxidation proceeds rapidly through chain propagation steps. The final plateau region indicates the depletion of C_2H_4 and increased radical-radical recombination, which reduces the net oxidation rate. As the lamp intensity increases from $\Phi = 9$ W to 20 W in Fig. 4(c), the lag phase shortens due to faster radical formation, but the recombination and photo-saturation effects become more pronounced. Consequently, the slope of the conversion curve decreases at high conversion. This behaviour signifies a transition from kinetically controlled to photonic-limited regimes, consistent with the fractional order observed at elevated light intensities by Mabusela et al. (2024).

4.3. Effect of humidity and hydroxyl radical generation

The Box-Behnken design (Tables 4 – 6) offers supporting experimental evidence of the effects of initial ethylene concentration, relative humidity and lamp power on percentage ethylene removal. These runs broaden the experimental coverage of the process variables, but they do not constitute independent validation of the deterministic model. The governing equations do not explicitly include humidity-dependent hydroxyl radical chemistry. The *ANOVA* in Table 6 shows that all three variables - initial concentration (X_1), humidity (X_2), and lamp wattage (X_3) - significantly affect percentage ethylene removal at $p < 0.001$, with X_1 and X_3 exerting the largest influence. Due to the difference in the units of the independent variables, a coded approach was used to standardise the range of variables, as shown in Table 4 and the experimental combinations are listed in Table 5. The resulting PER estimate from coded data is given by:

$$PER = 22.22 - 32.07x_1 + 11.23x_2 + 15.43x_3 - 5.55x_1x_2 - 12.40x_1x_3 + 8.80x_2x_3 + 21.04x_1^2 + 3.89x_2^2 - 2.56x_3^2 \quad (23)$$

Figs. 5 and 6 demonstrate that moderate humidity enhances PER at low concentration and low power, whereas excessive humidity

Table 4
The factors and levels used in the Box-Behnken design of experiment.

Level	Code	Independent Variables		
		X_1: $[C_2H_4]_0$ (ppm)	X_2: Humidity (%)	X_3: Power (W)
Max. level	+1	50	90	9
Central level	0	27.5	45	6
Min. level	-1	5	0	3

Table 5
Experimental results of the Box-Behnken design for the effect of humidity, lamp wattage and initial C_2H_4 concentration on the percentage ethylene removal (PER).

Run	Coded variables			Actual C_2H_4 removed (%)	Predicted C_2H_4 removed (%)
	x_1	x_2	x_3		
1	0	+1	-1	13.5	10.55
2	-1	0	+1	100	100
3	+1	+1	0	17.2	20.75
4	-1	-1	0	66	62.45
5	0	0	0	20.6	22.22
6	0	0	0	19.5	22.22
7	+1	-1	0	5.4	9.4
8	+1	0	-1	6.2	5.6
9	-1	0	-1	38	44.95
10	+1	0	+1	18.6	11.65
11	0	-1	-1	9.1	5.7
12	0	+1	+1	55.6	59
13	0	-1	+1	16	18.95
14	0	0	0	21.5	22.22
15	-1	+1	0	100	96
16	0	0	0	29.4	22.22
17	0	0	0	20.1	22.22

Table 6
Analysis of Variance (ANOVA) for photolysis of C_2H_4.

Source	*SS*	*DF*	*MS*	*F*-value	*p*-value
Model	14165.12	9	1573.90	42.11	< 0.0001
X_1 - Initial [C_2H_4]	8230.45	1	8230.45	220.20	< 0.0001
X_2 – Humidity	1008.00	1	1008.00	26.97	0.0013
X_3 – Wattage	1903.44	1	1903.44	50.92	0.0002
X_1X_2	123.21	1	123.21	3.30	0.1123
X_1X_3	615.04	1	615.04	16.45	0.0048
X_2X_3	309.76	1	309.76	8.29	0.0237
X_1^2	1863.92	1	1863.92	49.87	0.0002
X_2^2	63.71	1	63.71	1.70	0.2330
X_3^2	27.59	1	27.59	0.7383	0.4187
Residual	261.64	7	37.38		
Lack of Fit	195.06	3	65.02	3.91	0.1106
Pure Error	66.59	4	16.65		
Total	14426.76	16			

suppresses removal efficiency at high concentration. This dual behaviour arises from competing mechanisms: (i) water vapour photolysis generates hydroxy radicals that accelerate oxidation (Feiyan et al., 2002), and (ii) excessive moisture inhibits the production of ozone and promotes radical recombination, reducing net photon flux (Cheng et al., 2011). These findings stress the need for humidity control to optimise both chemical and photonic efficiency. The quadratic response surface model in Eq. 23 provided a good statistical fit, with an overall *F*-value of 42.11 and non-significant lack of fit ($p = 0.1106$). The predicted versus observed PER values yielded $R^2 = 0.982$, indicating that the selected process variables capture most of the measurable variability; and RMSE = 3.92%, demonstrating low deviation between experimental observation and model predictions. The parity plot illustrating the reliability of the model across the investigated range is presented in Fig. 7. The mean residual was found to be −0.035%, indicating negligible systematic deviation. Furthermore, the 95% confidence interval for the residuals was calculated as [-2.11%, 2.04%], which includes zero. This confirms that the model predictions are statistically unbiased.

4.4. Cost optimisation

Fig. 8 is a plot of the operational cost of the VUV photolysis reactor under the conditions summarised in Tables 1 and 2. The cost profile exhibits an initial gradual decline followed by a rapid drop to a distinct minimum, beyond which the cost increases proportionally with lamp power. This profile is consistent with the reaction phases within the reactor. In the lag phase, the cost associated with unreacted C_2H_4 decreases slightly as radicals begin to form and conversion remains low. During propagation phase, enhanced radical availability leads to pronounced decrease in unreacted C_2H_4 cost and a minimum in total costs. In the recombination phase, radical quenching and photon-saturation effects limit further conversion, and the operational cost is dominated by the electrical power consumption of the lamp. An optimum occurs where the marginal benefit of additional degradation equals the marginal energy expense. In Fig. 8, the minimal treatment cost is shown to be a strong function of the lamp wattage, with the absolute value decreasing with increasing lamp power. For a lamp wattage of 9 W this cost was determined to be approximately 0.6% of the retail value, indicating that VUV photolysis can be economically viable for high-value perishable commodities.

The use of a spoilage coefficient k_s to quantify ethylene-related losses introduces an important link between reactor physics and postharvest economics, a feature not reported in previous VUV studies. This framework thus enables reactor design based on total cost per ethylene-removed unit rather than conversion efficiency alone, advancing practical deployment of photolysis in cold-storage operations.

5. Conclusion

This study presents a coupled mass-energy balance and cost optimization model for ethylene degradation in a VUV photolysis reactor. The model reproduces the measured temperature response at the single validation condition (9 W and 90% RH), but shows underprediction of conversion at longer reaction times. The latter discrepancy limits the model's quantitative applicability under the tested high humidity condition and is consistent with the omission of explicit hydroxyl-radical

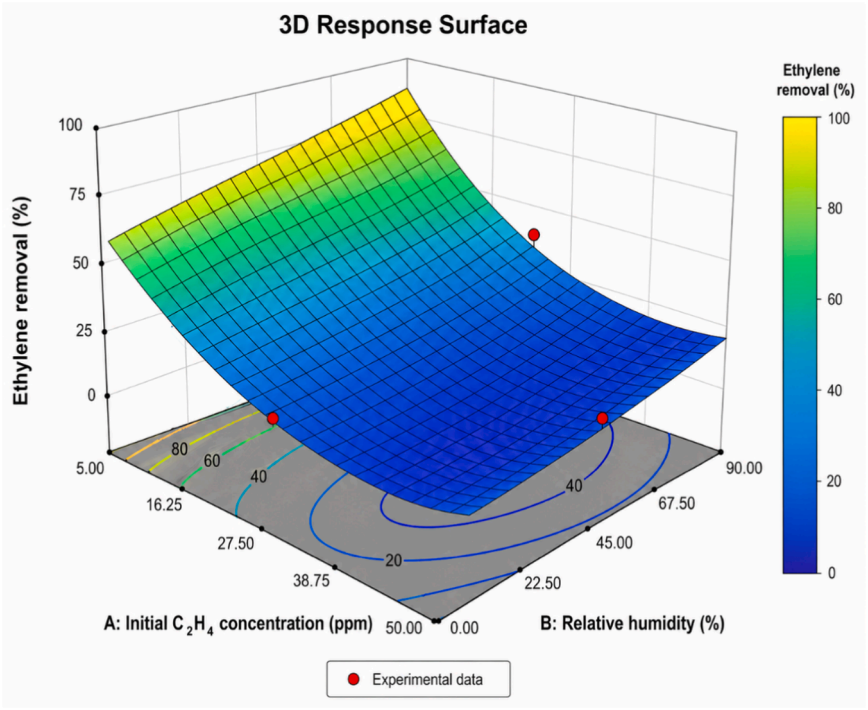


Fig. 5. Response surface illustrating the interaction between humidity and initial ethylene concentration on percentage ethylene removal at 3 W.

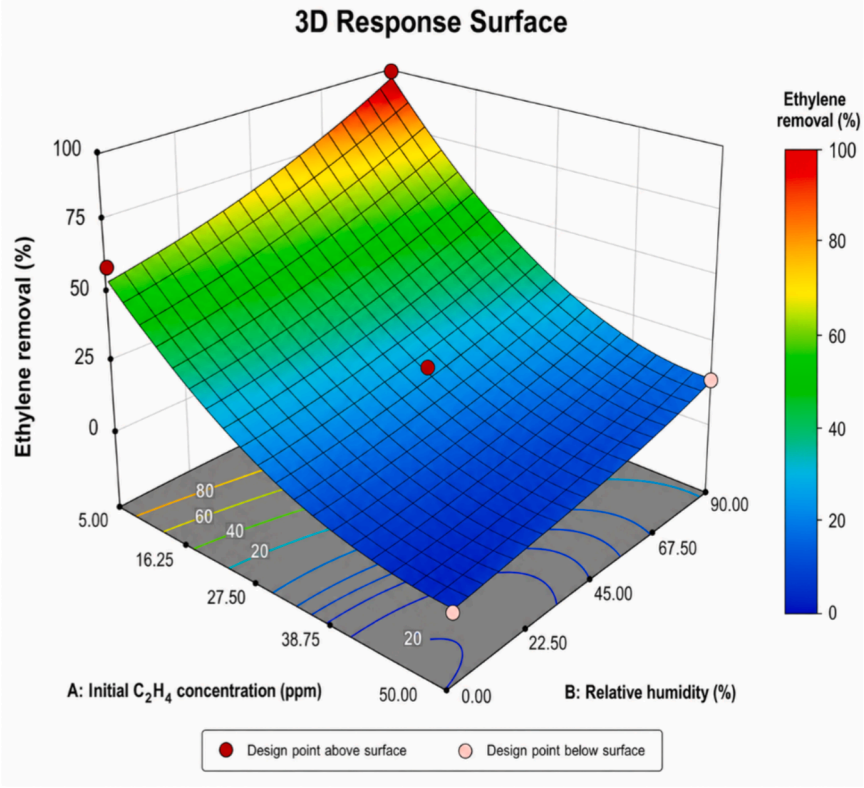


Fig. 6. Response surface illustrating the interaction between humidity and initial ethylene concentration on percentage ethylene removal at 6 W.

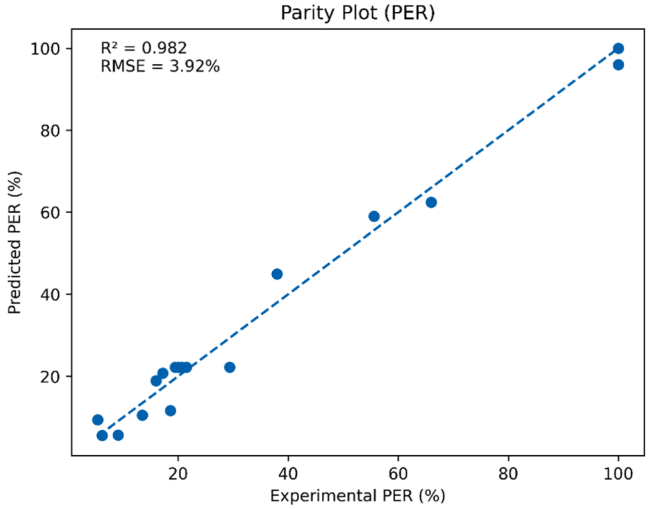


Fig. 7. Parity plot comparing predicted and experimental percentage ethylene removal (PER) obtained from the RSM model.

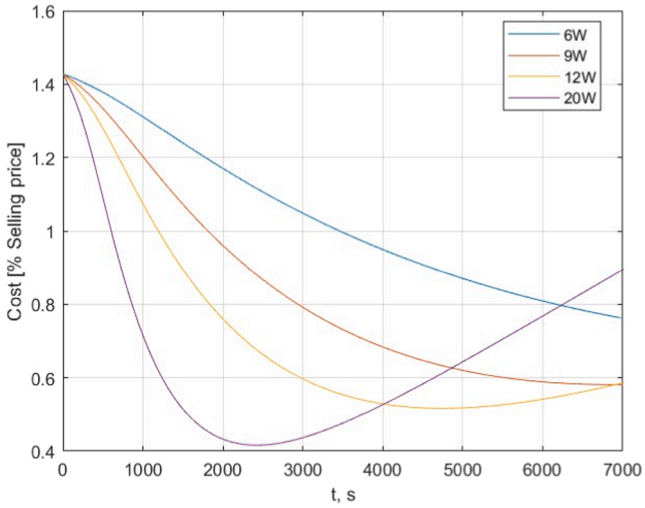


Fig. 8. Operational costs of VUV photolysis reactor for C_2H_4 oxidation.
List of Tables.

chemistry. The Box-Behnken experiments provide supporting evidence that relative humidity, initial ethylene concentration and lamp power affect ethylene removal, but are not independent validation of the deterministic model. Integration of thermal, kinetic, and economic aspects provides a unified framework for assessing process performances and cost-effectiveness. Economic analysis revealed an optimum operation point which minimises the running costs of electricity while maintaining an acceptable rate of conversion of C_2H_4, demonstrating feasibility for industrial postharvest applications.

By coupling reactor physics with postharvest economics, this study advances the quantitative design of energy-efficient VUV photolysis systems. Future work should focus on extending the model to continuous reactors, incorporating spectral radiative transfer and hydroxyl radical kinetics.

CRediT authorship contribution statement

Buntu Godongwana: Writing – review & editing, Supervision, Resources, Formal analysis. **Nina Mntwini:** Writing – original draft, Investigation, Conceptualization. **Bongolwetu Mabusela:** Validation, Investigation. **Patricia Mathabe:** Validation, Conceptualization.

Declaration of Competing Interest

The authors declare that they have no known competing financial interest or personal relationships that could have appeared to influence the work reported in this paper.

Acknowledgement

Funding: This work was supported by the National Research Foundation (NRF) of South Africa (Grant number TTK200412512752), awarded to Dr Godongwana.

Appendix A

$$\sum_{i=1}^{6}\Omega_i=\frac{\alpha_1\Pi_0}{\theta}(1-x_C)+\frac{\alpha_2K_2}{\theta^2}(1-x_C)(b_1-x_C)+\frac{\alpha_3\Pi_1}{\theta}(1-x_B)+\frac{\alpha_4K_4}{\theta^2}(1-x_D)(b_2-x_D)e^{-\zeta_4/\theta}+\frac{\alpha_5K_5}{\theta^2}(1-x_A)(b_3-x_A)e^{-\zeta_5/\theta}+\frac{\alpha_6K_6}{\theta^2}(1-x_A)(b_4-x_A)e^{-\zeta_6/\theta} \tag{A1}$$

The constants K_i, b_i are given by:

$$K_2=\frac{k_2c_Mc_{C0}}{k_0};K_4=\frac{k_{40}c_{D0}}{k_0};K_5=\frac{k_{50}c_{A0}}{k_0};K_6=\frac{k_{60}c_{A0}}{k_0} \tag{A2}$$

$$b_1=\frac{c_{D0}}{c_{C0}};b_2=\frac{c_{B0}}{c_{D0}};b_3=\frac{c_{D0}}{c_{A0}};b_4=\frac{c_{B0}}{c_{A0}} \tag{A3}$$

The corresponding α_i constants:

$$\alpha_1=\frac{c_{C0}H_{rxn,1}}{\rho c_pT_0};\alpha_2=\frac{c_{C0}H_{rxn,2}}{\rho c_pT_0};\alpha_3=\frac{c_{B0}H_{rxn,3}}{\rho c_pT_0};\alpha_4=\frac{c_{D0}H_{rxn,4}}{\rho c_pT_0};\alpha_5=\frac{c_{A0}H_{rxn,5}}{\rho c_pT_0};\alpha_6=\frac{c_{A0}H_{rxn,6}}{\rho c_pT_0} \tag{A4}$$

Data availability

Data will be made available on request.

References

Asili, V., de Visscher, A., 2014. Mechanistic model for ultraviolet degradation of H_2S and NO_x in waste gas. Chem. Eng. J. 244, 597–603. https://doi.org/10.1016/j.cej.2014.01.078.

Asili, V., de Visscher, A., 2018. Modelling methane and ethane photolysis in waste gas: optimization of reaction networks. Can. J. Chem. Eng. 96 (8), 1674–1683. https://doi.org/10.1002/cjce.23124.

Atkinson, R., 1997. Gas-phase tropospheric chemistry of volatile organic compounds: 1. Alkanes and Alkenes. J. Phys. Chem. Ref. Data. 26, 215–290. https://doi.org/10.1063/1.556012.

Atkinson, R., Baulch, D.L., Cox, R.A., Crowley, J.N., Hampson, R.F., Hynes, R.G., Jenkin, M.E., Rossi, M.J., Troe, J., 2004. Evaluated kinetic and photochemical data for atmospheric chemistry: Volume I – gas phase reactions of O_x, HO_x, NO_x and SO_x species. Atmos. Chem. Phys. 4, 1461–1738. https://doi.org/10.5194/acp-4-1461-2004.

Atkinson, R., Baulch, D.L., Cox, R.A., Crowley, J.N., Hampson, R.F., Hynes, R.G., Jenkin, M.E., Rossi, M.J., Troe, J., 2006. Evaluated kinetic and photochemical data for atmospheric chemistry: Volume II – gas phase reactions of organic species. Atmos. Chem. Phys. 6, 3625–4055. https://doi.org/10.5194/acp-6-3625-2006.

Bagheri, M., Mohseni, M., 2014. Computational fluid dynamics (CFD) modelling of VUV/UV photoreactors for water treatment. Chem. Eng. J. 256, 51–60. https://doi.org/10.1016/j.cej.2014.06.068.

Chang, K.-L., Sekiguchi, K., Wang, Q., Zhao, F., 2013. Removal of ethylene and secondary organic aerosols using UV-$C_{254+185nm}$ with TiO2 catalyst. Aerosol Air Qual. Res. 13, 618–626. https://doi.org/10.4209/aaqr.2012.07.0195.

Chen, J.-M., Cheng, Z.-W., Jiang, Y.-F., Zhang, L.-L., 2010. Direct VUV photodegradation of gaseous α-pinene is a spiral quartz reactor: Intermediates, mechanism, and toxicity/biodegradability assessment. Chemosphere 81, 1053–1060. https://doi.org/10.1016/j.chemosphere.2010.09.060.

Cheng, Z.-W., Jiang, Y.-F., Zhang, L.-L., Chen, J.-M., Wei, Y.-Y., 2011. Conversion characteristics and kinetic analysis of gaseous -pinene degraded by a VUV light in various reaction media. Sep. Purif. Technol. 77, 26–32. https://doi.org/10.1016/j.seppur.2010.11.014.

Cvetanović, R.J., 1987. Evaluated chemical kinetic data for the reactions of atomic oxygen $O(^3P)$ with unsaturated hydrocarbons. J. Phys. Chem. Ref. Data. 16 (2), 261–326. https://doi.org/10.1063/1.555783.

FAO, 2024. Rome. World Food and Agriculture – Statistical Yearbook 2024. FAO. https://doi.org/10.4060/cd2971en.

Farkas, L., Monzini, I., Takács, E., Wojnárovits, L., Vörös, M., Vágvölgyi, C., Janáky, C., Alapi, T., 2024. Comparison of the effectiveness of UV, UV/VUV photolysis, ozonation, and ozone/UV processes for the removal of sulfonamide antibiotics. J. Environ. Chem. Eng. 12, 111845. https://doi.org/10.1016/j.jece.2023.111845.

Feiyan, C., Pehkonen, S.O., Ray, M.B., 2002. Kinetics and mechanisms of UV-photodegradation of chlorinated organics in the gas phase. Water Res. 36, 4203–4214. https://doi.org/10.1016/S0043-1354(02)00140-9.

Huang, H., Lu, H., Huang, H., Wang, L., Zhang, J., Leung, D.Y.C., 2016. Recent development of VUV-based processes for air pollutant degradation. Front. Environ. Sci. 4 (17), 1–13. https://doi.org/10.3389/fenvs.2016.00017.

Jozwiak, Z.B., Bartsch, J.A., Aneshansley, D.J., 2000. Modelling disappearance of ethylene from controlled storage atmospheres exposed to ultraviolet radiation. Agric. 2000 Int. Conf. Model. Control. Agric. Hortic. Post. -Harvest. Process. July 10-12th. Wagening. Neth. https://doi.org/10.1016/S1474-6670(17)40914-1.

Keller, N., Ducamp, M.-N., Robert, D., Keller, V., 2013. Ethylene Removal and Fresh Product Storage: A challenge at the Frontiers of Chemistry. Toward an Approach by Photocatalytic Oxidation. Chem. Rev. 113 (7), 5029–5070. https://pubs.acs.org/doi/10.1021/cr900398v.

Khan, S., Alvi, A.F., Saify, S., Iqbal, N., Khan, N.A., 2024. The Ethylene Biosynthetic Enzymes, 1-Aminocyclopropane-1-Carboxylate (ACC) Synthase (ACS) and ACC Oxidase (ACO): The Less Explored Players in Abiotic Stress Tolerance. Biomolecules 14 (90), 1–34. https://doi.org/10.3390/biom14010090.

Klöpffer, W., Wagner, B.O., 2007. Weinheim. Atmospheric Degradation of Organic Substances. Wiley.

Levenspiel, O., 1998. Chemical Reaction Engineering, 3rd ed. Wiley, New Jersey.

Mabusela, B.P., Belay, Z.A., Godongwana, B., Caleb, O.J., 2023. Impact of vacuum ultraviolet (VUV) photolysis on ethylene degradation kinetics and removal in mixed-fruit storage, and direct exposure to 'Fuji' apples during storage. J. Food Sci. Technol. 60, 2557–2567. https://doi.org/10.1007/s13197-023-05775-3.

Mabusela, B.P., Belay, Z.A., Godongwana, B., Pathak, N., Mahajan, P.V., Caleb, O.J., 2022. Advances in vacuum ultraviolet photolysis in the postharvest management of fruit and vegetables along the value chains: a review. Food Bioprocess. Technol. 15, 28–46. https://doi.org/10.1007/s11947-021-02703-1.

Mabusela, B.P., Godongwana, B., Belay, Z.A., Caleb, O.J., 2024. Ethylene degradation via vacuum ultraviolet photolysis: nth-order kinetic model, energy consumption assessment, and a case study for 'Fuji' apples under retail conditions. Food Bioprod. Process. 147, 230–238. https://doi.org/10.1016/j.fbp.2024.07.006.

Mahmoudkhani, F., Rezaei, M., Asili, V., Atyabi, M., Vaisman, E., Langford, C., de Visscher, A., 2016. Benzene degradation in waste gas by photolysis and photolysis-ozonation: experiments and modelling. Front. Env. Sci. Eng. 10, 1–10. https://doi.org/10.1007/s11783-016-0876-4.

Nasir, U., Ismail, A., Riaz, M., Razzaq, K., Ali, S., Hussain, A., Ameen, M., Saif, A., Aslam, F., de Oliveira, C.A.F., 2024. Exploring fruit ripening methods: conventional, artificial, and novel approaches for quality and health. Food Control. 165, 110626. https://doi.org/10.1016/j.foodcont.2024.110626.

Pathak, N., Caleb, O.J., Rauh, C., Mahajan, P.V., 2017. Effect of process variables on ethylene removal by vacuum ultraviolet radiation: application in fresh produce storage. Biosyst. Eng. 159, 33–45. https://doi.org/10.1016/j.biosystemseng.2017.04.008.

Pathak, N., Caleb, O.J., Rauh, C., Mahajan, P.V., 2019. Efficacy of photocatalysis and photolysis systems for the removal of ethylene under different storage conditions. Postharvest Biol. Technol. 147, 68–77. https://doi.org/10.1016/j.postharvbio.2018.09.006.

Pathak, N., Mahajan, P.V., 2017. Ethylene Removal from Fresh Produce Storage: Current Methods and Emerging Technologies. Geoff Smithers (ed). 2017. Reference Module in Food Science. Elsevier, Amsterdam. https://doi.org/10.1016/B978-0-08-100596-5.22330-5.

Popiel, C.O., 2008. Free convection heat transfer from vertical slender cylinders: A review. Heat. Transf. Eng. 29 (6), 521–536. https://doi.org/10.1080/01457630801891557.

Ray, M.B., 2000. Photodegradation of the Volative Organic Compounds in the Gas Phase: A Review. Dev. Chem. Eng. Miner. Process. 8, 405–439. https://doi.org/10.1002/apj.5500080502.

Soneji, I.B., Bakane, P.H., Mohod, V.D., Bisen, R.D., Khobragade, U.H., 2024. Ethylene management strategies for fresh produce preservation: A comprehensive review. Int. J. Adv. Biochem. Res. 8 (12), 1110–1120. https://doi.org/10.33545/26174693.2024.v8.i12Sn.3305.

Wang, J.H., Ray, M.B., 2000. Application of ultraviolet photooxidation to remove organic pollutants in the gas phase. Sep. Purif. Technol. 19, 11–20. https://doi.org/10.1016/S1383-5866(99)00078-7.

Warneck, P., 1988. Chemistry of the Natural Atmosphere. In: International Geophysics Series, 41. Academic Press, New York.

Xu, J.-H., Ding, B.-B., Lv, X.-M., Lan, S.-H., Li, C.-L., Peng, L., 2018. Mathematical Modeling and Mechanism of VUV Photodegradation of H_2S in the Absence of O_2 (Article ID). Int. J. Photo, 2769213. https://doi.org/10.1155/2018/2769213.